CONDENSED
MATTER
PHYSICS

Regular article

Anomalous thermodynamics of a quantum spin system with large residual entropy

J. Richter[1,2], J. Schulenburg[3], D. V. Dmitriev[4], V. Ya. Krivnov[4], J. Schnack[5]

[1] Institut für Physik, Otto-von-Guericke-Universität Magdeburg, P.O. Box 4120, 39016 Magdeburg, Germany

[2] Max-Planck-Institut für Physik komplexer Systeme, Nöthnitzer Straße 38, 01187 Dresden, Germany

[3] Universitätsrechenzentrum, Universität Magdeburg, D-39016 Magdeburg, Germany

[4] Institute of Biochemical Physics of RAS, Kosygin Street 4, 119334 Moscow, Russia

[5] Fakultät für Physik, Universität Bielefeld, Postfach 100131, 33501 Bielefeld, Germany

September 15, 2020

By contrast to strongly frustrated classical systems their quantum counterparts typically have a non-degenerate ground state. A counterexample is the celebrated Heisenberg sawtooth spin chain with ferromagnetic zigzag bonds J_1 and competing antiferromagnetic basal bonds J_2. At a quantum phase transition point $|J_2/J_1| = 1/2$ this model exhibits a flat one-magnon excitation band leading to a massively degenerate ground-state manifold which results in a large residual entropy. Thus, for the spin-half model the residual entropy amounts to exactly one half of its maximum value $\lim_{T\to\infty} S(T)/N = \ln 2$. In the present paper we study in detail the role of the spin quantum number s and the magnetic field H in the parameter region around the transition (flat-band) point. For that we use full exact diagonalization up to $N = 20$ lattice sites as well as the finite-temperature Lanczos method up to $N = 36$ sites to calculate the density of states as well as the temperature dependence of the specific heat, the entropy and the susceptibility. The study of chain lengths up to $N = 36$ allows a careful finite-size analysis. At the flat-band point we find extremely small finite-size effects for spin $s = 1/2$, i.e., the numerical data virtually correspond to the thermodynamic limit. In all other cases the finite-size effects are still small and become visible at very low temperatures. In a sizeable parameter region around the flat-band point the influence of the former massively degenerate ground-state manifold acts as a large manifold of low-lying excitations leading to extraordinary thermodynamic properties at the transition point as well as in the vicinity of it, such as an additional low-temperature maximum in the specific heat. Moreover, there is a very strong influence of the magnetic field on the low-temperature thermodynamics including an enhanced magnetocaloric effect.

Key words: *quantum Heisenberg model, frustration, sawtooth chain, residual entropy*

PACS: *75.10.-b, 75.10.Jm*

1. Introduction

The sawtooth chain is one of the paradigmatic frustrated quantum spin models built of corner-sharing triangles. The corresponding Heisenberg Hamiltonian is given by

$$\mathcal{H} = J_1 \sum_{\langle i,j \rangle} \mathbf{s}_i \cdot \mathbf{s}_j + J_2 \sum_{\langle\langle i,j \rangle\rangle} \mathbf{s}_i \cdot \mathbf{s}_j - H \sum_i S_i^z \tag{1.1}$$

with $\mathbf{s}_i^2 = s(s+1)$. Here the first sum runs over the zigzag bonds and the second one over the basal bonds, see figure 1. There are numerous studies of this spin model, see, e.g., references [1–24] within different contexts ranging from exact dimer product ground states [1, 3, 4, 14] via quantum three-coloring description [17, 18, 23] to many-body quantum scars [24]. As a prototype of a flat-band model the sawtooth chain has attracted particular attention by the community investigating frustrated quantum spin systems, see, e.g., references [2, 9, 10, 12, 13, 15, 16, 19, 21, 23] as well as by groups studying electronic systems, see, e.g., references [25–33], and also
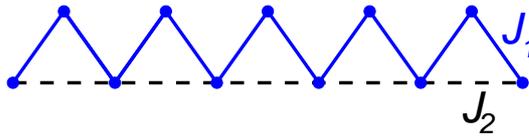
Figure 1. A schematic picture of the sawtooth chain.

photonic lattices, see, e.g. references [34, 35]. Further motivation for theoretical studies comes from several magnetic compounds where the magnetic ions reside on sawtooth lattice sites, see, e.g. references [36–40].

The focus of the present paper is on a specific version of the sawtooth Heisenberg model with ferromagnetic (FM) zigzag bonds $J_1 < 0$ and competing antiferromagnetic (AFM) basal bonds $J_2 > 0$. We will call this model the FM-AFM sawtooth chain. This model undergoes a quantum phase transition at $\kappa_c = |J_2/J_1| = 1/2$ from a FM to a ferrimagnetic ground state [7, 11, 15], where κ_c is independent of the spin quantum number s [15]. At the transition (flat-band) point κ_c, the lowest one-magnon excitation band above the FM state becomes flat and it has zero energy [15, 16, 19, 22, 23]. Such a flat one-magnon band leads to a massively degenerate set of localized multi-magnon ground states resulting in an s-independent residual entropy $\lim_{N \to \infty} S_0(N)/N = \frac{1}{2} \ln 2$ [15], which is even larger than for the AFM sawtooth chain at its flat-band point [9, 10]. While the thermodynamics of the AFM sawtooth chain is well studied see, e.g., references [9, 10, 12, 13, 41], so far only a few investigations are available for the FM-AFM sawtooth chain [15, 16, 19, 22, 23]. Since the flat-band physics for this model can be observed at zero field it might be even more interesting than the AFM model, where flat-band physics appears around the saturation field, i.e., typically at high magnetic fields. Therefore, by contrast to the FM-AFM sawtooth chain, the high-field flat-band physics for purely AFM models is not easily (or not at all) accessible in experiments, for the few exceptions see references [42–46]. A strong further motivation to extend the theoretical study of the FM-AFM sawtooth chain comes from the recently synthesized magnetic molecule $Gd_{10}Fe_{10}$ [38]. This magnetic system is well described by the FM-AFM sawtooth chain with of $10 + 10$ alternating gadolinium ($S = \frac{7}{2}$) and iron ($S = \frac{5}{2}$) ions, sitting on apical and basal sites, correspondingly. Importantly, the ratio of its exchange parameters is close to the transition point [16, 19, 38]. We further mention that the model is also relevant for $Cs_2LiTi_3F_{12}$ that hosts ferro-antiferromagnetic sawtooth chains as magnetic subsystems [47].

Here we present a systematic study of the role of the system size N, the spin quantum number s as well the change of the thermodynamic properties in dependence on the distance to the transition point $d_f = |J_2/J_1| - \kappa_c$. Moreover, we also discuss the influence of the magnetic field on the thermodynamics, which may have a strong impact on the low-temperature physics, because it lifts partially the huge degeneracy present at $|J_2/J_1| = \kappa_c$. For that we use full exact diagonalization (ED) and the finite-temperature Lanczos method (FTLM).

2. Methods

2.1. Full exact diagonalization (ED)

The exact-diagonalization technique is a powerful numerical tool which is widely applied to quantum lattice models, see, e.g. reference [48]. Using a complete set of basis states the stationary Schrödinger equation for a finite system of N sites is transformed to an eigenvalue problem. Then the full spectrum can be determined by numerical diagonalization without approximations. We use here Jörg Schulenburg's *spinpack* code [49, 50] which allows to treat periodic $s = 1/2$ sawtooth chains up to $N = 20$ sites easily.

2.2. Finite-temperature Lanczos method (FTLM)

The FTLM is a Monte-Carlo like extension of the full ED briefly described in the previous section. Thermodynamic quantities are determined using trace estimators [51–61]. The partition function Z is approximated by a Monte-Carlo like representation of Z, i.e., the sum over a complete set of $(2s + 1)^N$ basis states entering Z is replaced by a much smaller sum over R random vectors $| \nu \rangle$ for each subspace $\mathcal{H}(\gamma)$ of the Hilbert space. To split the Hilbert space into small subspaces we use conservation of total S^z as well as the lattice symmetries of the Hamiltonian, where the mutually orthogonal subspaces are labeled by γ. The exponential of the Hamiltonian

is approximated by its spectral representation in a Krylov space spanned by the N_L Lanczos vectors starting from the respective random vector $|v\rangle$. Then the FTLM approximation of the partition function is given by

$$Z(T) \approx \sum_{\gamma=1}^{\Gamma} \frac{\dim(\mathcal{H}(\gamma))}{R} \sum_{v=1}^{R} \sum_{n=1}^{N_L} \exp\left(-\frac{\epsilon_n^{(v)}}{kT}\right) |\langle n(v) | v \rangle|^2. \tag{2.1}$$

Here $|n(v)\rangle$ is the nth eigenvector of $\mathcal{H}$ in the Krylov space with the corresponding energy $\epsilon_n^{(v)}$. As for ED we use for the numerical Lanczos calculations J. Schulenburg's *spinpack* code [49, 50] to get FTLM data for periodic sawtooth chains up to $N = 36$ sites.

3. Results

3.1. The model at the flat-band point

Let us first recapitulate some important results found in reference [15]. Due to the characterization of the ground-state manifold by localized multi-magnon (LMM) states explicit expressions for the degeneracies in each S_z-sector were found. For periodic spin-half chains with N sites the ground-state degeneracy at the transition point in a particular S_z-sector with $S^z = S_{\max} - k$ is

$$D_N^k = \frac{n!}{(n-k)!(k)!}, \quad 0 \leq k \leq \frac{n}{2}, \; n = \frac{N}{2}$$

$$D_N^k = \frac{n!}{(n/2)!(n/2)!} + \delta_{k,n}, \quad \frac{n}{2} < k \leq n . \tag{3.1}$$

That yields the total degeneracy

$$D_N = 2^n + n\frac{n!}{(n/2)!(n/2)!} + 1 , \; n = \frac{N}{2} \tag{3.2}$$

leading to a residual entropy per site $s_0 = \lim_{N\to\infty} \frac{1}{N} \ln D_N = \frac{1}{2} \ln 2$. Note that this value is independent of s (for $N \to \infty$ only) and it corresponds to a system of $N/2$ independent spin-half objects. Interestingly, the excitation gap Δ above the ground-state manifold is extremely small. Thus, for $N = 20$ the ED yields $\Delta = 7.502 \cdot 10^{-9}$. Moreover, Δ decreases with increasing N. Thus, the FM-AFM sawtooth chain at $|J_2/J_1| = \kappa_c$ is a (rare) example of a virtually gapless finite quantum spin system.

Applying a magnetic field $H > 0$, the fully polarized state with $S_z = S_{\max} = Ns$ becomes the ground state and the former LMM ground states of the other S_z-sectors are excited states, where their excitation energy is related to the Zeeman term. Because of their huge degeneracy, see equation (3.1), this class of excitations may dominate the low-temperature physics. Thus the contribution of the LMM states to the partition function can be explicitly given, see equation (27) in reference [15]. Based on this knowledge universal scaling relations for the magnetization and the susceptibility were found. For the susceptibility the universal finite-size scaling function reads [15]

$$\chi_N(T) = T^{-\alpha} f(c_N N T^{\alpha-1}), \tag{3.3}$$

where the N-dependent factor c_N (given by a cumbersome formula) becomes $c_N = 1/48$ for $N \gg 1$ and the scaling exponent α for $s = 1/2$ was determined to $\alpha \simeq 1.09$ by fitting to corresponding finite-size data for $N = 16$ and $N = 20$. Below we will verify this scaling behavior by comparing corresponding finite-size data for much larger systems up to $N = 36$.

3.1.1. Density of states

Before we will present our numerical data for thermodynamic quantities such as the specific heat $c(T)$ and the susceptibility $\chi(T)$ we will briefly illustrate in more detail the low-energy spectrum by discussing the excitation gaps and the density of states $\rho(E)$. In Table 1 we present ED data for the excitation gaps in different sectors of $S^z = Ns - k$ for $N = 16$ and spin $s = 1/2, 1, 3/2$ and 2. Obviously, the gaps are rather small if $k > 1$, where the

Table 1. Excitation gaps $\Delta(k) \equiv E_1(k) - E_0$ of the periodic FM-AFM sawtooth chain of $N = 16$ sites at the transition point $|J_2/J_1| = 1/2 = \kappa_c$, $J_1 = -1$, for spin quantum numbers $s = 1/2, 1, 3/2$ and 2 in different subspaces $S^z = Ns - k$. $E_1(k)$ is the energy of the lowest excitation in the subspace of k magnons and $E_0 = -12s^2$ is the ground-state energy.

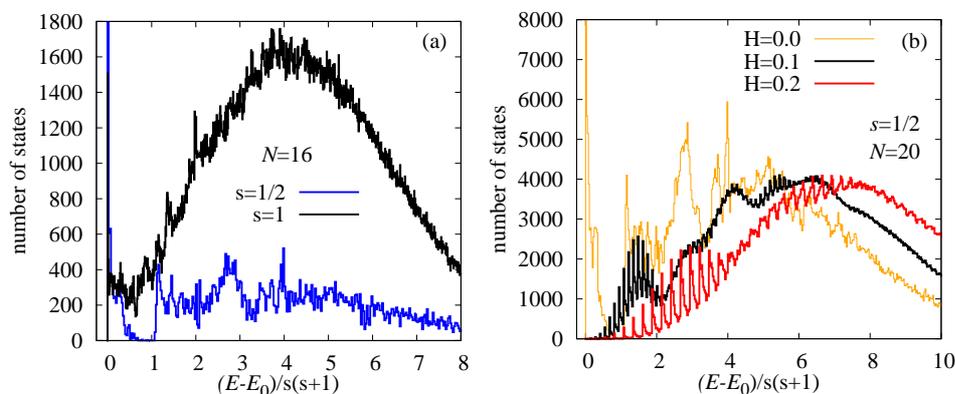|	$s = 1/2$	$s = 1$	$s = 3/2$	$s = 2$
k	$\Delta(k)$	$\Delta(k)$	$\Delta(k)$	$\Delta(k)$
1	1.0	2.0	3.0	4.0
2	$2.178 \cdot 10^{-2}$	$7.094 \cdot 10^{-2}$	$8.596 \cdot 10^{-2}$	$9.326 \cdot 10^{-2}$
3	$4.718 \cdot 10^{-4}$	$4.829 \cdot 10^{-3}$	$6.902 \cdot 10^{-3}$	$7.924 \cdot 10^{-3}$
4	$9.935 \cdot 10^{-6}$	$2.740 \cdot 10^{-4}$	$4.797 \cdot 10^{-4}$	$5.917 \cdot 10^{-4}$
5	$3.034 \cdot 10^{-6}$	$1.550 \cdot 10^{-4}$	$2.682 \cdot 10^{-4}$	$3.248 \cdot 10^{-4}$
6	$2.584 \cdot 10^{-6}$	$1.550 \cdot 10^{-4}$	$2.682 \cdot 10^{-4}$	$3.248 \cdot 10^{-4}$
7	$7.361 \cdot 10^{-7}$	$1.550 \cdot 10^{-4}$	$2.682 \cdot 10^{-4}$	$3.248 \cdot 10^{-4}$

Figure 2. (a) Density of states (histogram, bar width $\Delta E = 0.02$) of periodic chains of $N = 16$ sites with $J_1 = -1$ and $J_2 = 1/2$ for spin $s = 1/2$ and $s = 1$ (ED), where the y-axis is cut at 1800. Note that within the first histogram bar between E_0 and $E_0 + \Delta E$ not only the ground states but also excited states are collected, see also Table 1. (b) Field dependence of the density of states (histogram, bar width $\Delta E = 0.02$) of periodic chains of $N = 20$ sites with $J_1 = -1$, $J_2 = 1/2$ and spin $s = 1/2$ (ED), where the y-axis is cut at 8000.

extreme quantum case plays a particular role with a virtually vanishing gap (see also Table I in reference [15] for $s = 1/2$ with $N = 16, 20, 24, 28$ and $k = 1, \ldots, 6$).

In figure 2(a) we show $\rho(E)$ for $N = 16$ and spin quantum numbers $s = 1/2$ and $s = 1$. An exceptional feature of the density of states for $s = 1/2$ is the collection of about 6% of the states in the low-energy region below $E - E_0 \lesssim 0.6$, where this region is separated by a quasi-gap from the high-energy region $E - E_0 \gtrsim 0.6$. This feature is present also for larger system sizes, see references [15] and [23]. The particular low-energy structure of $\rho(E)$ is important for the low-temperature physics, see below. As can be also seen in figure 2(a) the separation of the low-energy part of the spectrum is much less pronounced for $s = 1$ and gradually vanishes as further increasing of s. Another peculiar feature of the spectrum of the $s = 1/2$ model is the absence of the expected typical maximum of the density of states in the middle of the spectrum.

The influence of a small magnetic field on the density of states is illustrated in figure 2(b) for $s = 1/2$ and $N = 20$. As already briefly discussed above, at $H > 0$ the ground state is the single fully polarized ferromagnetic state and the degeneracy of the different S_z sectors is lifted. However, the degeneracy of the LMM states within a certain S_z sector, see equation (3.1), is still present leading to the unconventional spiked structure of $\rho(E)$ below $(E - E_0)/s(s + 1) \lesssim 2$ for $H = 0.1$ and below $(E - E_0)/s(s + 1) \lesssim 4$ for $H = 0.2$, where the location of the peaks corresponds to the Zeeman energy of the respective S_z sector. These parts of the spectrum related to
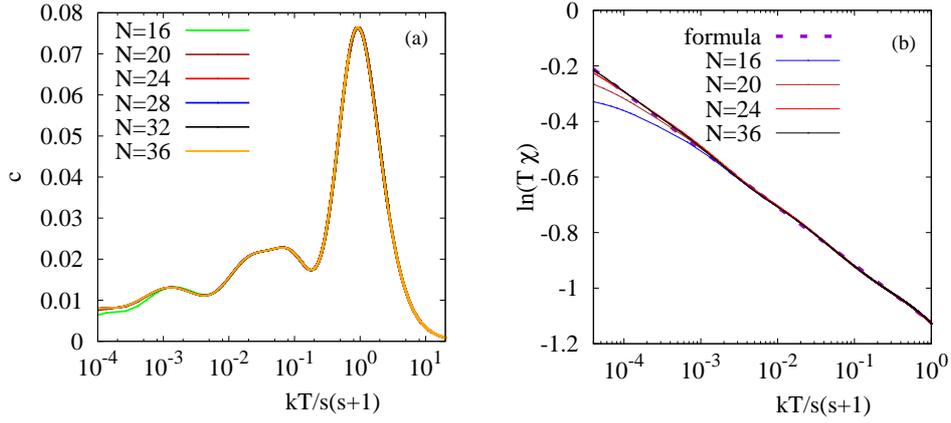
Figure 3. (a) Specific heat $c(T)$ per site of periodic chains of $N = 16, 20, 24, 28, 32, 36$ sites with $J_1 = -1$, $J_2 = 1/2$ and spin $s = 1/2$ (ED for $N = 16, 20$, FTLM for $N = 24, 28, 32, 36$) at zero magnetic field. (b) Log-log plot for the dependence of the susceptibility per site on temperature for periodic chains of $N = 16, 20$ (ED) and $N = 24, 36$ (FTLM) with $J_1 = -1$, $J_2 = 1/2$ and spin $s = 1/2$. The symbols correspond to the formula $\chi(T) = 0.317/T^{1.09}$.

the LMM states will dominate the low-temperature properties.

3.1.2. Specific heat, entropy and uniform susceptibility

Similar as for the energy scale of the density of states we use for the thermodynamic quantities the normalized temperature $T/s(s + 1)$ to get a better comparison between systems of different s. (Note that the temperature dependences of the specific heat $c(T)$ as well as for the susceptibility $\chi(T)$ for different s become identical at high temperatures as a function of $T/s(s + 1)$ [63].)

In reference [15], by comparing data for $N = 16, 18, 20, 22$ for the $s = 1/2$ sawtooth chain, it was found (i) that the low-temperature part is very specific with a long tail down to very low temperatures including two weak additional maxima below the typical main maximum and (ii) that the finite-size effects seem to be very small. It is also worth mentioning that the unconventional low-temperature part of $c(T)$ below the main maximum is entirely covered by the energy levels below the quasi-gap, cf. reference [23].

We strengthen these statements by including FTLM data up to $N = 36$, see figure 3(a), where we show the specific heat at the transition point for spin $s = 1/2$. Obviously, there are no finite-size effects down to $T/s(s + 1) \sim 0.0001$ (only for the smallest system of $N = 16$ we see small deviations from the curves for larger N at $T < 0.001$). We also observe, that the FTLM approximation is very accurate, cf. reference [60]. Thus our finite-size data for spin $s = 1/2$ virtually correspond the thermodynamic limit. This feature can be attributed to the virtually vanishing excitation gaps, cf. Sec. 3.1.1. For the temperature dependence of the susceptibility, which is related to equation (3.3), in reference [15] the formula $\chi(T) = 0.317/T^{1.09}$ was found. In figure 3(b) we show $\ln(T\chi)$ vs. $T/s(s + 1)$ for $N = 16, 20, 24, 36$. Obviously, the finite-size effects are again small and the curves for $N = 24$ and 36 perfectly coincide with the above given formula for $\chi(T)$ in the whole temperature region shown in figure 3(b). Thus the data for larger N further confirm equation (3.3). It turns out that the scaling exponent α present in the scaling function equation (3.3) depends on the spin quantum number s [22]. It changes from $\alpha = 1.09$ for the extreme quantum case $s = 1/2$ to $\alpha = 1.23$ for $s = 1$ and then it smoothly tends to $\alpha = 1.5$ at $s \to \infty$.

We consider now the sawtooth chain with higher spin s. In figure 4(a) and (b) we show the specific heat and the entropy for $N = 12$ and spin values $s = 1/2, 1, 3/2, 2, 5/2, 3$. As for $s = 1/2$, for all $s > 1/2$ we observe a long tail below the main maximum reaching to very low temperatures. However, by contrast to the extreme quantum case $s = 1/2$, the low-temperature part does not exhibit additional maxima rather there is a shoulder just below the main maximum. The position $T_{max}/s(s + 1)$ and the height c_{max} of the main maximum in $c(T)$ strongly depend on s, see the inset of figure 4(a). Obviously, the maximum moves to smaller values of $T/s(s + 1)$ as increasing of s. From the exact solution of the classical case [19] it is known that for $s \to \infty$ there
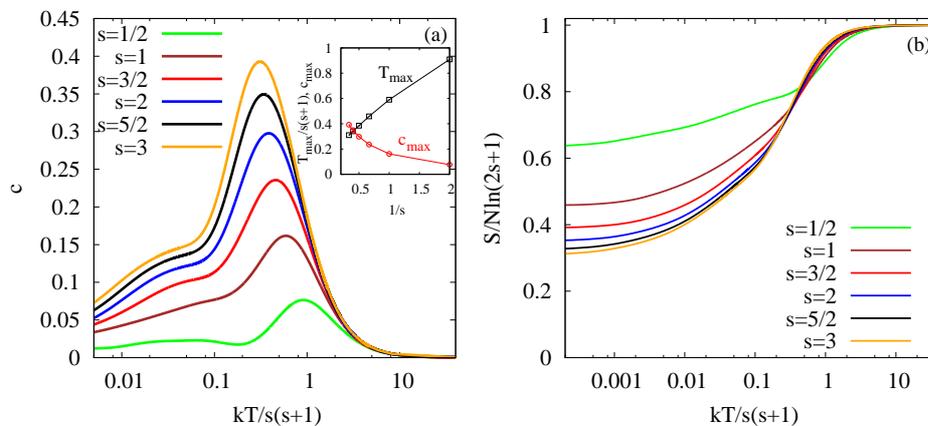
Figure 4. (a): Main panel: Specific heat $c(T)$ per site of periodic chains of $N = 12$ sites with $J_1 = -1$, $J_2 = 1/2$ for spin $s = 1/2, 1, 3/2, 2, 5/2, 3$ at zero magnetic field. Inset: Position $T_{\max}/s(s+1)$ and height $c_{\max}$ of the main maximum in $c(T)$ as a function of the inverse spin quantum number s. (b): Scaled entropy $s(T)/N \ln(2s+1)$ per site for $N = 12$ sites with $J_1 = -1$, $J_2 = 1/2$ for spin $s = 1/2, 1, 3/2, 2, 5/2, 3$ at zero magnetic field.
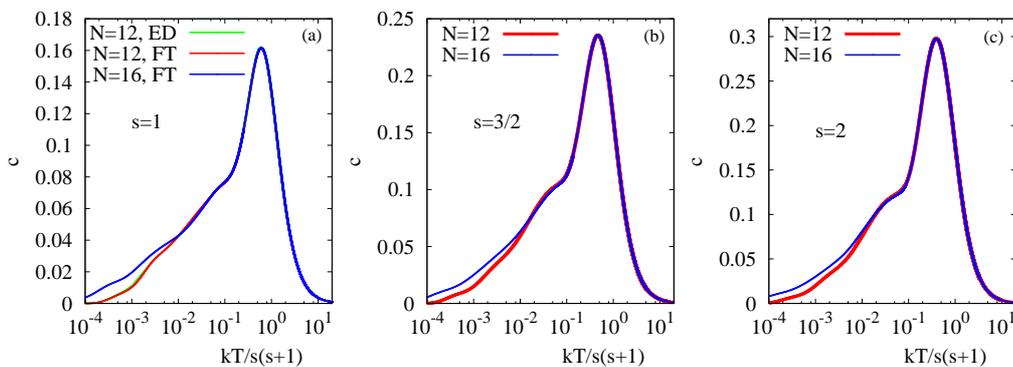

Figure 5. (a) Specific heat $c(T)$ per site for periodic chains of $N = 12$ and 16 sites with $J_1 = -1$, $J_2 = 1/2$ and spin $s = 1$ (ED for $N = 12$, FTLM for $N = 12$ and $N = 16$) at zero magnetic field. (b)-(c) Same as in (a) but without ED for s = 3/2 and 2, respectively.
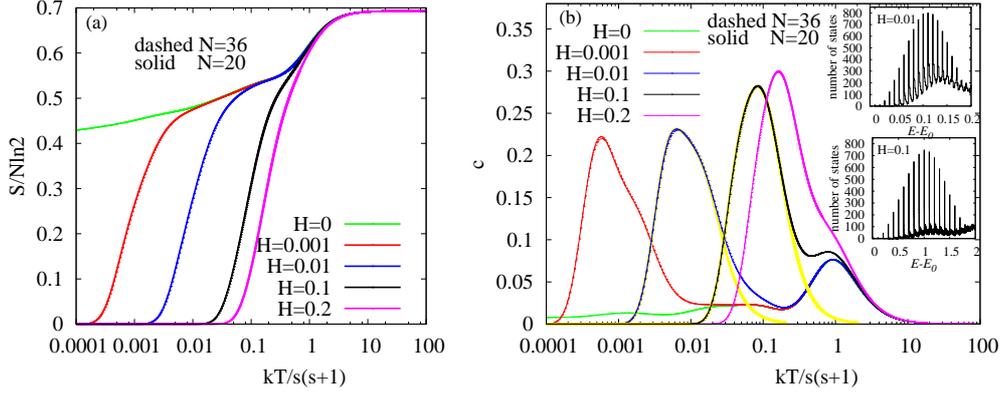
Figure 6. (a) Scaled entropy $s(T)/N \ln(2s+1)$ per site for periodic chains of $N = 20$ (ED) and 36 (FTLM) sites with $J_1 = -1$, $J_2 = 1/2$ and spin $s = 1/2$ for various magnetic fields H. (Note that the curves for $N = 20$ and $N = 36$ coincide, i.e., the dashed lines are practically not visible.) (b) Main panel: Influence of the magnetic field H on the specific heat $c(T)$ per site for periodic chains of $N = 20$ (ED - solid) and $N = 36$ (FTLM - dashed) sites with $J_1 = -1$, $J_2 = 1/2$ and spin $s = 1/2$. (Note that the curves for $N = 20$ and $N = 36$ perfectly coincide, i.e., the dashed lines are practically not seen.) The broad yellow curves are calculated using a restricted set of energies to determine the specific heat, namely $E < E_0 + 0.15$ ($E < E_0 + 1.5$) for $H = 0.01$ ($H = 0.1$). Inset: Density for states for $H = 0.01$ and $H = 0.1$ shown for that energy region relevant for the extra low-temperature maximum in $c(T)$ presented in the main panel.

is no maximum, rather the $c(T)$ exhibits a plateau-like shape with $c(T < T_p) > 0$, $T_p/s(s+1) \sim 0.2$. We may conclude, while for most spin systems the low-T thermodynamics for the pretty large spin value $s = 3$ is close to the classical case, the highly frustrated FM-AFM sawtooth chain is an example, where $s = 3$ is still far from the classical limit. For all considered values of s the general entropy profiles (figure 4 (b)) are similar, however, with different values of the residual entropy. The slow convergence towards the classical limit as increasing of s may be related to the exponentially large ground state degeneracy.

According to the larger excitation gaps for $s > 1/2$, see Table 1, we may expect that finite-size effects set in earlier as $T \to 0$. In figure 5 (a), (b), (c) we show the specific heat at the flat-band point $\kappa_c = |J_2/J_1| = 1/2$ for spin $s = 1$, $s = 3/2$ and $s = 2$ and $N = 12$ and $N = 16$. Finite-size effects become visible below the shoulder, i.e., at about $kT/s(s+1) < 0.01$, but the general shape of the $c(T)$ curve remains similar as increasing N.

3.1.3. Influence of the magnetic field

As briefly discussed for the density of states (see Sec. 3.1.1) a magnetic field may have a drastic influence on the low-energy physics by partial lifting the massive ground-state degeneracy. Here we focus on the specific heat $c(T)$ and the entropy $s(T)$. The magnetization process has been recently studied in detail in reference [22].

We present numerical data for $s(T)$ and $c(T)$ for $N = 20$, $N = 36$ and $s = 1/2$ in figure 6(a) and (b), respectively, where magnetic fields $H = 0$, 0.001, 0.01, 0.1, 0.2 are considered. The lifting of the massive ground-state degeneracy by the magnetic field is well visible in figure 6(a). There is no residual entropy at $H > 0$, however, by increasing the temperature, at small fields the entropy $s(H, T)$ approaches the zero-field value $s(H = 0, T)$ (green line in figure 6(a)) pretty fast.

At small nonzero field $H \lesssim 0.121$ the specific heat exhibits a fairly high low-temperature maximum. This maximum is caused by a series of low-lying excitations stemming from the former degenerate LMM zero-field ground states, see the well separated sharp peaks in the density of states shown in the inset of figure 6(b). This becomes evident by the broad yellow curves which are determined using a restricted set of energies to compute the specific heat. Clearly, the position of the low-temperature maximum $T_{\max}(H)$ is related to the Zeeman energies of the LMM states and it is approximately given by $T_{\max} = 0.615H$. Again, finite-size effects are negligible.
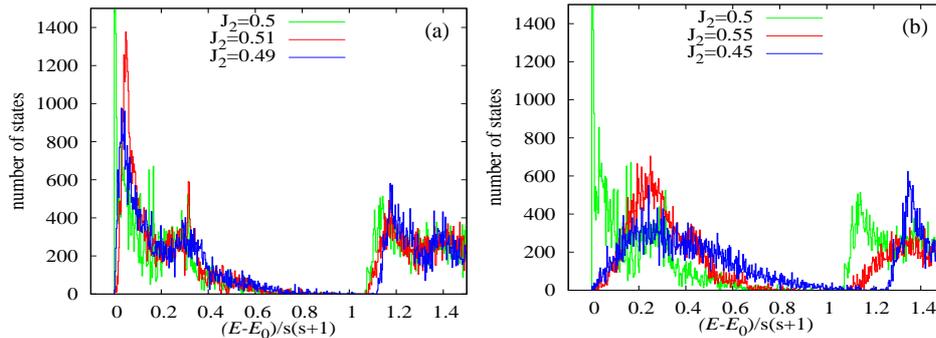
Figure 7. Low-energy part of the density of states (histogram, bar width $\Delta E = 0.002$) of periodic $s = 1/2$ chains of $N = 20$ sites with $J_1 = -1$ and (a) $J_2 = 0.49$ and $J_2 = 0.51$ as well as (b) $J_2 = 0.45$ and $J_2 = 0.55$ compared with the density of states at the flat-band point ($J_2 = 0.5$). Note that the y-axis is cut at 1500.
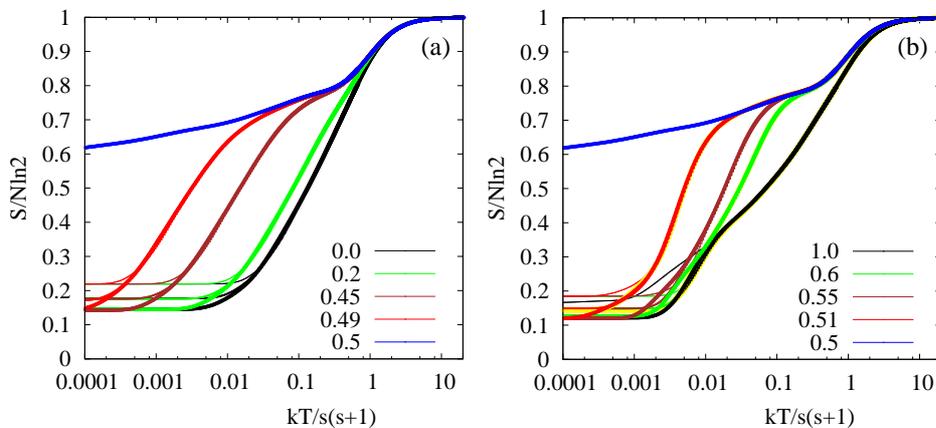

Figure 8. Scaled entropy $S(T)/N \ln 2$ per site of periodic chains of $N = 20, 28, 36$ sites [$N = 20$ (ED) - thin, $N = 28$ (FTLM) - middle, $N = 36$ (FTLM) - thick] for spin $s = 1/2$, $J_1 = -1$ and various values of (a) $J_2 \leq \kappa_c$ and (b) $J_2 \geq \kappa_c$ (the J_2 values are given in the legend) at zero magnetic field.

3.1.4. Signatures of flat-band physics away from the flat-band point κ_c

The realization of the ideal flat-band physics in an experiment on a sawtooth magnet is unlikely. Rather, one may expect that in a specific magnetic compound the exchange parameters are sufficiently close to the flat-band point. A striking example is the FM-AFM sawtooth-chain magnetic molecule $Gd_{10}Fe_{10}$ [38], where the ratio of exchange parameters J_1 and J_2 is slightly below the flat-band point. However, the Gd and Fe ions carry large spins s and the system of $N = 20$ spins is not accessible by ED or FTLM. Hence, we focus here on spin $s = 1/2$ that again allows the analysis of finite-size effects for $|J_2/J_1| \neq \kappa_c$ by considering various N up to $N = 36$.

The LMM states stemming from the flat-band are exact eigenstates only at the flat-band point. Moving away from this point the states and thus also the eigenvalues are modified. As result the massive ground-state degeneracy is lifted and the majority of the former LMM states become a large manifold of low-lying excitations. One may expect that the change of energies is smooth, where the excitation energies depend on the distance from the flat-band point $d_f = |J_2/J_1| - \kappa_c$.

We start with the discussion of the density of states $\rho(E)$, see figure 7, where we show the low-energy part of $\rho(E)$ for several values of J_2. The lifting of the ground-state degeneracy as well as the low-energy manifold of the former LMM ground states and the energy shift of them with growing $d_f = |J_2/J_1| - \kappa_c$ is evident. Moreover, the quasi-gap is still present and the states below the quasi-gap determine the low-temperature physics.

The specific features of the low-energy spectrum lead to a specific behavior of the entropy shown in figure 8.
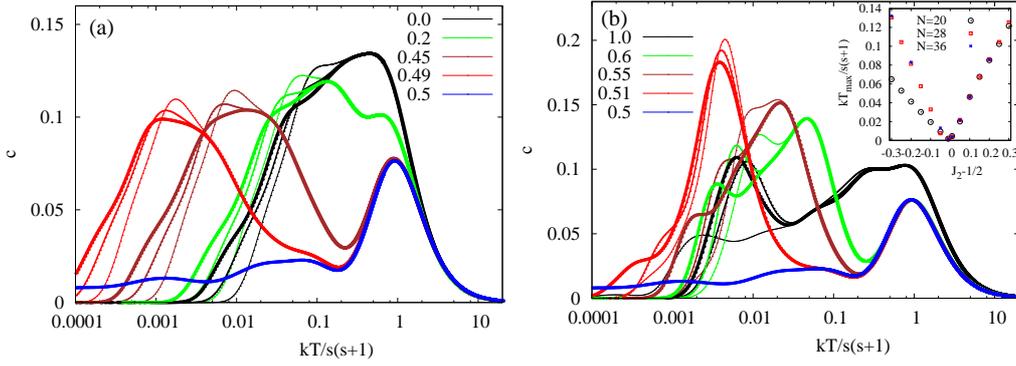
Figure 9. Main panel: Specific heat per site of periodic chains of $N = 20, 28, 36$ sites [$N = 20$ (ED) - thin, $N = 28$ (FTLM) - middle, $N = 36$ (FTLM) - thick] for spin $s = 1/2$, $J_1 = -1$ and various values of (a) $J_2 \leq \kappa_c$ and (b) $J_2 \geq \kappa_c$ (the J_2 values are given in the legend) at zero magnetic field. The inset in panel (b) shows the position of the low-temperature maximum of $c(T)$ as a function of the distance to the transition point $d_f = |J_2/J_1| - \kappa_c$.

There is only a small residual entropy related to the ferromagnetic (ferrimagnetic) ground-state multiplet at $J_2 < 1/2$ ($J_2 > 1/2$), which vanishes as $\ln N/N$ when $N \to \infty$. This size-dependent residual entropy yields the splitting of the curves for various N at low T. By increasing the temperature, at small deviations from the flat-band point the entropy approaches the flat-band value $s(J_2 = 1/2, T)$ (blue line in figure 8).

The specific heat $c(T)$ is shown in figure 9(a) and (b) for a few values below and above the flat-band point κ_c. Apparently, $c(T)$ exhibits clear signatures of flat-band physics in a sizeable parameter region below and above κ_c, namely a well-pronounced low-temperature peak coming from the former LMM ground states. On the other hand, the main peak is quite stable against small deviations from κ_c. Noticeable finite-size effects set in around the low-temperature peak, i.e., only at very low temperatures. The position of the low-temperature peak T_{max} depends on the energy-shift of the LMM states, i.e., on the distance from the flat-band point d_f, see the inset in figure 9(b). For $d_f > 0$, there is a linear relation $T_{max} \approx 0.33 d_f$, $0 < d_f \lesssim 0.3$, where the finite-size effects are small. On the other hand, for $d_f < 0$ the peak position is noticeably dependent on N, but there is no doubt of the double-maximum structure in the $c(T)$ profile.

Last but not least, we briefly discuss the magnetic cooling. There are several theoretical studies reporting an enhanced magnetocaloric effect in the vicinity of a quantum phase transition, in particular if there is a residual entropy at the transition point, see, e.g., references [6, 9, 12, 64–66]. However, most of the previous studies in flat-band systems report on an enhanced magnetocaloric effect near the saturation field [6, 9, 12, 64–66], which often is not accessible in experiments. By contrast, the FM-AFM sawtooth chain exhibits this phenomenon when approaching zero field [15] which is more promising thinking in terms of a possible experimental realization. In figure 10 we show as an example the temperature variation as a function of the applied magnetic field for an isentropic cooling with fixed entropy $S/N = 0.5$ for spin $s = 1/2$ and $N = 36$ and various values of J_2. Apparently, there is a noticeable downturn in the $T(H)$ curve as $H \to 0$ for values of J_2 in the vicinity of the flat-band point, indicating the presence of an enhanced magnetocaloric effect in the FM-AFM sawtooth chain.

4. Summary

In the present paper we study finite spin-s Heisenberg sawtooth chains with ferromagnetic (FM) zigzag bonds $J_1 < 0$ and competing antiferromagnetic (AFM) basal bonds $J_2 > 0$ by means of full exact diagonalization and the finite-temperature Lanczos method. The model exhibits at $\kappa_c = |J_2/J_1| = 1/2$ a zero-temperature transition between a ferro- and a ferrimagnetic ground state. At the transition (flat-band) point κ_c, the lowest one-magnon excitation band above the ferromagnetic state is flat (dispersionless) and has zero energy. This leads to a massively degenerate ground-state manifold resulting in a residual entropy $\lim_{N \to \infty} S_0(N)/N = \frac{1}{2} \ln 2$, that is independent of s. Moreover, in the extreme quantum case $s = 1/2$ already for the finite systems of up to $N = 36$ sites the excitations above the ground-state manifold are virtually gapless with the result that the finite-size data
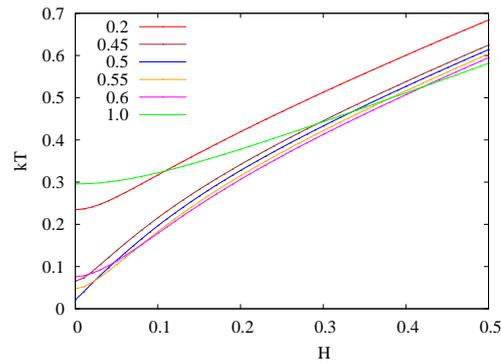
Figure 10. Temperature in dependence on the applied magnetic field for an isentropic cooling with fixed entropy $S/N = 0.5$ for spin $s = 1/2$ and $N = 36$ and various values of J_2 (given in the legend). Corresponding data for $N = 20$ (not shown) demonstrate that finite-size effects are small.

practically correspond to the thermodynamic limit.

For spin quantum numbers $s > 1/2$ the quantum effects at low temperatures remain strong, even for the largest spin $s = 3$ considered here. Thus, at the flat-band point the specific-heat profile exhibits a well-pronounced maximum with a shoulder-like part and long tail down to very low temperatures below this maximum for all $s = 1, \ldots, 3$, whereas this feature is not present in the classical case.

In a sizeable parameter region around the flat-band point the influence of the former massively degenerate ground-state manifold acts as a large manifold of low-lying excitations setting an extra low-energy scale yielding unconventional low-temperature thermodynamics which can be understood as a remnant of flat-band physics.

A specific feature of the flat-band system at hand is the strong influence of an applied magnetic field on the low-temperature properties caused by a partial lifting of degenerate ground-state manifold, i.e., most states collected in the residual entropy at zero field become low-energy excitations according to their Zeeman energy.

Finally we argue that our results for the FM-AFM Heisenberg sawtooth chain might be (at least to some extent) representative for other systems with a large residual entropy such as the three-coloring XXZ sawtooth chain [17, 18, 23] and the FM-AFM kagome chain [67].

Acknowledgments

References

1. D. Sen, B. S. Shastry, R. E. Walstedt, and R. Cava, Phys. Rev. B, 1996, **53**, 6401.
2. J. Schulenburg, A. Honecker, J. Schnack, J. Richter, and H.-J. Schmidt, Phys. Rev. Lett., 2002. **88**, 167207.
3. S. Chen, H. Büttner, and J. Voit, Phys. Rev. B, 2003, **67**, 054412.
4. S.A. Blundell and M. D.Nunez-Regueiro, Eur. Phys. J. B, 2003, **31**, 453.
5. S.A. Blundell and M. D.Nunez-Regueiro, J. Phys.: Condens. Matter, 2004, **16**, S791.
6. M. E. Zhitomirsky and A. Honecker, J. Stat. Mech.: Theor. Exp., 2004, P07012.
7. T. Tonegawa and M. Kaburagi, J. Magn. Magn. Mater., 2004, **272-276**, 898.
8. V.R. Chandra, D. Sen, N.B. Ivanov, and J. Richter, Phys. Rev. B, 2004, **69**, 214406.
9. M.E. Zhitomirsky and H. Tsunetsugu, Phys. Rev. B, 2004, **70**, 100403.
10. O. Derzhko and J. Richter, Phys. Rev. B, 2004, **70**, 104415.
11. M. Kaburagi, T. Tonegawa, and M. Kang, J. Appl. Phys., 2005, **97**, 10B306.
12. O. Derzhko and J. Richter, Eur. Phys. J. B, 2006, **52**, 23.

13. J. Richter, O. Derzhko, and A. Honecker, Int. J. Mod. Phys. B, 2008, **22**, 4418.
14. Z. Hao, Y. Wan, I. Rousochatzakis, J. Wildeboer, A. Seidel, F. Mila, and O. Tchernyshyov, Phys. Rev. B, 2011, **84**, 094452.
15. V. Ya. Krivnov, D.V. Dmitriev, S. Nishimoto, S.-L. Drechsler, and J. Richter, Phys. Rev. B, 2014, **90**, 014441.
16. D. V. Dmitriev and V. Ya. Krivnov, Phys. Rev. B, 2015, **92**, 184422.
17. H. J. Changlani, D. Kochkov, K. Kumar, B. K. Clark, and E. Fradkin, Phys. Rev. Lett., 2018 **120**, 117202.
18. H. J. Changlani, S. Pujari, C.-M. Chung, and B. K. Clark, Phys. Rev. B, 2019, **99**, 104433.
19. D. V. Dmitriev, V. Ya. Krivnov, J. Richter, and J. Schnack, Phys. Rev. B, 2019, **99**, 094410.
20. T. Yamaguchi, S.-L. Drechsler, Y. Ohta, and S. Nishimoto, Phys. Rev. B, 2020, **101**, 104407.
21. A. Metavitsiadis, C. Psaroudaki, and W. Brenig, Phys. Rev. B, 2020 **101**, 235143.
22. D. V. Dmitriev, V. Ya. Krivnov, J. Schnack, and J. Richter, Phys. Rev. B, 2020, **101**, 054427.
23. O. Derzhko, J. Schnack, D. V. Dmitriev, V. Ya. Krivnov and J. Richter, Eur. Phys. J. B, 2020, **93**, 161.
24. P. A. McClarty, M. Haque, A. Sen, and J. Richter, arXiv:2007.01311.
25. H. Tasaki, Phys. Rev. Lett., 1992, **69**, 1608.
26. A. Mielke, H. Tasaki, Commun. Math. Phys., 1993, **158**, 341.
27. H. Tasaki, J. Stat. Phys., 1996, **84**, 535.
28. Y. Watanabe and S. Miyashita, J. Phys. Soc. Jpn., 1997, **66**, 2123.
29. R. Arita, Y. Shimoi, K. Kuroki, and H. Aoki, Phys. Rev. B, 1998, **57**, 10609.
30. O. Derzhko, J. Richter, A. Honecker, M. Maksymenko, and R. Moessner, Phys. Rev. B, 2010, **81**, 014421.
31. M. Maksymenko, A. Honecker, R. Moessner, J. Richter, and O. Derzhko, Phys. Rev. Lett., 2012, **109**, 096404.
32. S. Flach, D. Leykam, J. D. Bodyfelt, P. Matthies, and A. S. Desyatnikov, EPL (Europhysics Letters), 2014, **105**, 30001.
33. W. Zhang, R. Liu, and W. Nie, Science Bulletin, 2019 **64**, 1490.
34. S. Weimann, L. Morales-Inostroza, B. Real, C. Cantillano, A. Szameit, and R. A. Vicencio, Opt. Lett., 2016, **41**, 2414.
35. L. Tang, D. Song, S. Xia, S. Xia, J. Ma, W. Yan, Yi Hu, J. Xu, D. Leykam, and Z. Chen, Nanophotonics, 2020, **9**, 1161.
36. C. Ruiz-Perez, M. Hernandez-Molina, P. Lorenzo-Luis, F. Lloret, J. Cano, and M. Julve, Inorg. Chem., 2000, **39**, 3845.
37. Y. Inagaki, Y. Narumi, K. Kindo, H. Kikuchi, T. Kamikawa, T. Kunimoto, S. Okubo, H. Ohta, T. Saito, M. Azuma, M. Takano, H. Nojiri, M. Kaburagi, and T. Tonegawa, J. Phys. Soc. Jpn., 2005, **74**, 2831.
38. A. Baniodeh, N. Magnani, Y. Lan, G. Buth, C. E. Anson, J. Richter, M. Affronte, J. Schnack, and A. K. Powell, npj Quantum Mater., 2018, **3**, 10.
39. L. Heinze, H. Jeschke, A. Metavitsiadis, M. Reehuis, R. Feyerherm, J.-U. Hoffmann, A. U. B. Wolter, X. Ding, V. Zapf, C. C. Moya, F. Weickert, M. Jaime, K. C. Rule, D. Menzel, R. Valenti, W. Brenig, and S. Süllow, arXiv:1904.07820.
40. H. Nhalil, R. Baral, B. O. Khamala, A. Cosio, S. R. Singamaneni, M. Fitta, D. Antonio, K. Gofryk, R. R. Zope, T. Baruah, B. Saparov, and H. S. Nair, arXiv:1905.01037.
41. O. Derzhko, J. Richter, and M. Maksymenko, Int. J. Mod. Phys. B, 2015, **29**, 1530007.
42. H. Kikuchi, Y. Fujii, M. Chiba, S. Mitsudo, T. Idehara, T. Tonegawa, K. Okamoto, T. Sakai, T. Kuwai, and H. Ohta, Phys. Rev. Lett., 2005, **94**, 227201..
43. A. Honecker, S. Hu, R. Peters, and J. Richter, J. Phys.: Condens. Matter, 2011, **23**, 164211.
44. R. Okuma, D. Nakamura, T. Okubo, A. Miyake, A. Matsuo, K. Kindo, M. Tokunaga, N. Kawashima, S. Takeyama, and Z. Hiroi, Nat. Commun., 2019, **10**, 1229.
45. H. Tanaka, N. Kurita, M. Okada, E. Kunihiro, Y. Shirata, K. Fujii, H. Uekusa, A. Matsuo, K. Kindo, and H. Nojiri, J. Phys. Soc. Jpn., 2014, **83**, 103701.
46. J. Richter, O. Krupnitska, V. Baliha, T. Krokhmalskii, and O. Derzhko, Phys. Rev. B, 2018, **97**, 024405.
47. R. Shirakami, H. Ueda, H. O. Jeschke, H. Nakano, S. Kobayashi, A. Matsuo, T. Sakai, N. Katayama, H. Sawa, K. Kindo, C. Michioka, and K. Yoshimura, Phys. Rev. B, 2019, **100**, 174401.
48. A.M. Läuchli, 'Numerical simulations of frustrated systems', in Introduction to Frustrated Magnetism, edited by F. Mila C. Lacroix, P. Mendels (Springer, Berlin,Heidelberg, 2011) p. 34.
49. J. Schulenburg, spinpack-2.59 , Magdeburg University (2019).
50. J. Richter and J. Schulenburg, Eur. Phys. J. B, 2010, **73**, 117.
51. J. Jaklic and P. Prelovsek, Phys. Rev. B, 1994, **49**, 5065.
52. J. Jaklic and P. Prelovsek, Adv. Phys., 2000, **49**, 1..
53. A. Hams and H. De Raedt, Phys. Rev. E, 2000, **62**, 4365.
54. J. Schnack and O. Wendland, Eur. Phys. J. B, 2010, **78**, 535.
55. P. Prelovsek and J. Bonca, 'Strongly correlated systems, numerical methods', (Springer, Berlin, Heidelberg, 2013) Chap. 'Ground State and Finite Temperature Lanczos Methods'.
56. O. Hanebaum and J. Schnack, Eur. Phys. J. B, 2014, **87**, 194.
57. B. Schmidt and P. Thalmeier, Phys. Rep. 2017, **703**, 1.
58. E. Pavarini, E. Koch, R. Scalettar, and R. M. Martin, eds., 'The physics of correlated insulators, metals, and superconductors', (2017) Chap. 'The Finite Temperature Lanczos Method and its Applications' by P. Prelovsek, ISBN 978-3-95806-224-5, http://hdl.handle.net/2128/15283.

59. J. Schnack, J. Schulenburg, and J. Richter, Phys. Rev. B, 2018, **98**, 094423.
60. J. Schnack, J. Richter, and R. Steinigeweg, Phys. Rev. Research, 2020, **2**, 013186.
61. K. Seki and S. Yunoki, Phys. Rev. B, 2020, **101**, 235115.
62. J. Schnack, J. Schulenburg, A. Honecker, and J. Richter, Phys. Rev. Lett., 2020, **125**, 117207.
63. A. Lohmann, H.-J. Schmidt, and J. Richter, Phys. Rev. B, 2014, **89**, 014415.
64. M. E. Zhitomirsky, Phys. Rev. B, 2003, **67**, 104421.
65. J. Schnack, R. Schmidt, and J. Richter, Phys. Rev. B, 2007, **76**, 054413.
66. B. Wolf, A. Honecker, W. Hofstetter, U. Tutsch, and M. Lang, Int. J. Mod. Phys. B, 2014, **28**, 1430017.
67. D. V. Dmitriev and V. Ya. Krivnov. J. Phys.: Condens. Matter, 2017, **29**, 215801.